J Solid State Electrochem (2010) 14:1293–1301
DOI 10.1007/s10008-009-0938-7

ORIGINAL PAPER

Effect of synthetical conditions, morphology, and crystallographic structure of MnO_2 on its electrochemical behavior

Yujuan Yang · Chengde Huang

Received: 16 July 2009 / Revised: 9 September 2009 / Accepted: 15 September 2009 / Published online: 2 October 2009
© Springer-Verlag 2009

Abstract Manganese dioxide nanostructures have been synthesized by hydrothermal synthetical method. The crystallographic structure, morphology, and electrochemical properties of obtained MnO_2 are examined by XRD, TEM, cyclic voltammetry, and galvanostatic charge–discharge tests. The results showed that the electrochemical properties of MnO_2 were strongly affected by the crystallographic structure and morphology. The controlling crystallographic structure of MnO_2 can be obtained by altering the molar ratio of $KMnO_4/MnSO_4$. The morphology was affected by the hydrothermal dwell time and temperature. The optimal synthetic conditions are as follows: the initial molar ratio of $KMnO_4/MnSO_4$ is 3:1, the reaction lasts 2 h at 120 °C, and the filling factor is 90%. In these prepared conditions, the MnO_2 with the maximum specific capacitance of 259 $F\,g^{-1}$ can be obtained. Prepared δ-MnO_2 has a good layer structure and exhibits nanoflower morphology. The XRD studies show that the crystalline degree of this sample is lower, and the average grain size is about 8.3 nm. These results indicate that the product may have potential applications in areas such as electrode materials of supercapacitor and other new storing energy system.

Keywords Manganese dioxide · Supercapacitor · Hydrothermal synthesis · Crystallographic structure

Introduction

Electrochemical capacitors are new storing energy systems between batteries and conventional capacitors. They generally exhibit high capacitance (per unit volume or mass), which is 20–200 times greater than that of convention capacitor. Compared with usual batteries, electrochemical capacitors have advantages of high specific power density, long cycle life, and high charge–discharge rate [1]. In electrochemical capacitors, various materials such as porous carbon, transition metal oxides, and conductive polymer were used as electrode materials. Of all the transition metal oxides as pseudocapacitor materials, the manganese oxide (MnO_2) is attracting wide attention due to its low cost, environmentally friendly property, and broad potential window nature [2]. Therefore, the MnO_2 has been extensively investigated for preparing pseudocapacitor with highest capacitance.

Various approaches have been used to fabricate manganese oxide, such as self-reacting microemulsion [3], precipitation [4], room-temperature solid reaction [5], sonochemical [6], and hydrothermal methods [7]. Among these synthetic methods, the hydrothermal synthesis approach is one of the most easily controlling techniques of liquid phase chemical synthesis of nanostructure materials. Manganese oxide with different nanoarchitectures, such as nanowire [8], nanorod [9], and nanobelt [10], has been prepared by properly choosing the temperature or time of hydrothermal reaction, the active fill level in the pressure vessel, and the solvent without any major structure-directing agents or temperature. Each kind of nanostructure MnO_2 can provide unique performances and applications (each structure has its own merits). Xu et al. [11]. synthesized α-MnO_2 hollow spheres and hollow urchins and studied the electrochemical capacitance performance. Subramanian et al. [9] investigated the effect of hydrothermal time on the nanostructure and pseudocapacitance properties of MnO_2. However, the role of other reaction factor, such as mole ratio of reactants, is not still clear. In this paper, the nanostructure MnO_2 has been synthesized by

Y. Yang · C. Huang (✉)
Department of Applied Chemistry, School of Chemical Engineering and Technology, Tianjin University, Tianjin 300072, People's Republic of China
e-mail: cdhuang@tju.edu.cn

a hydrothermal route under mild conditions. The effects of reaction time, mole ratio of reactants, and reaction temperature on the crystallographic structure, morphology, and capacitance properties of MnO_2 are studied.

Experimental

Synthesis of MnO_2

All chemicals used in this experiment were analytical pure. In a typical procedure [9], the well-mixed aqueous solution of $KMnO_4$ and hydrated $MnSO_4$ were transferred to a Teflon-lined pressure vessel, which sealed and loaded into an oven preheated to 120 or 140 °C. The dwell time for the reaction had been varied from 1 to 18 h in order to optimize the material for electrochemical applications. Then, the pressure vessel was allowed to cool to room temperature naturally after the dwell time at 120 or 140 °C. The precipitate formed was filtered and washed with distilled water and ethanol to remove the unreacted materials. The water wash was done until the pH was 7. The precipitated MnO_2 was dried at 80 °C in air. The MnO_2 sample was obtained after grinding.

When the samples were obtained according to the following mode, the MnO_2 can be labeled as a1, a2, a3, a4, and a5: The reaction lasts for 6 h at 120 °C, the filling factor is 75%, and the initial molar ratio of $KMnO_4/MnSO_4$ is 1:1, 1.5:1, 2:1, 2.5:1 and 3:1, respectively.

When the samples were obtained according to following mode, the MnO_2 can be labeled as b1, b2, b3, b4, and b5: The initial molar ratio of $KMnO_4/MnSO_4$ is 2:1, the filling factor is 75%, and the reaction lasts for 2, 4, 6, 8, and 10 h at 120 °C, respectively.

When the samples were obtained according to following mode, the MnO_2 can be labeled as c1, c2, c3, and c4: The initial molar ratio of $KMnO_4/MnSO_4$ is 3:1, the filling factor is 90%, and the reaction lasts for 2, 6, 8, and 14 h at 120 °C, respectively.

When the samples were obtained according to following mode, the MnO_2 can be labeled as d1, d2, and d3: The initial molar ratio of $KMnO_4/MnSO_4$ is 2:1, the filling factor is 75%, and the reaction lasts for 6 h at 120, 130, or 140 °C, respectively.

Materials characterization

The X-ray diffraction measurements were performed on a Rigaku D/max 2,500 V X-ray diffractiometer with a Cu K_α (λ=1.5418 Å) radiation source, from 10° to 70° (2θ), using steps of 0.13° (2θ) and a step time of 1 s. The morphology of sample was examined with transition electron microscope (TEM, JEOL JEM-100CXII, Japan). The TEM specimen was prepared via the following procedure: Some samples were dispersed in anhydrous ethanol with ultrasonic vibration for 5 min; a drop of the supernatant was then transferred onto a standard holey carbon-covered copper TEM grid.

Preparation of electrode

The working electrode was prepared by inserting an active paste, which contained 70 wt% synthesized MnO_2, 25 wt% acetylene black, and 5 wt% polytetrafluorene-ethylene binder, into a nickel foam substrate. Small amount of ethanol was added to the mixture to produce more homogeneous paste by ultrasound for 30 min. The mixture dispersion was hand-brushed to nickel foam. The electrode was dried at room temperature and pressed under 14 MPa.

Electrochemical measurement

Eletcrochemical characterization was carried out in a conventional three-electrode cell. Platinum foil and saturated calomel electrode (SCE) were used as counter and reference electrode, respectively. Cyclic voltammetry (CV) and galvanostatic charge–discharge studies were performed using a CHI 660B electrochemical workstation (Chenhua Inc., Shanghai, China) between −0.2 and 1.0 V (vs. SCE) in a 0.5 mol L^{-1} Na_2SO_4 electrolyte. The specific capacitance can be calculated from the following equation [6]:

$$C_{\mathrm{m}} = \frac{i\Delta t}{m\Delta V} \tag{1}$$

where i is the galvanostatic charge–discharge current density applied, ($\Delta V/\Delta t$) is the slope of the charge–discharge plot, and m is the mass of the MnO_2 material.

Results

XRD studies

The structural framework of MnO_2 consists of basic MnO_6 octahedra units, which are linked in different ways to produce different crystallographic forms. The cumulative evidence published thus far established that the electrochemical performance of MnO_2 critically depends not only on its crystal structure and surface properties but also greatly on its textural properties including morphology, surface area, etc. [12–14]. These factors are influenced by reaction conditions, such as temperature, time, and pressure.

Figure 1 shows the X-ray diffraction (XRD) patterns of MnO_2 prepared at different reactant molar ratios, temperatures, and reaction time. It can be seen from Fig. 1a that the diffraction patterns of MnO_2 are similar with that at the molar ratio of $KMnO_4$ to $MnSO_4$, which is 1:1 and 2:1,

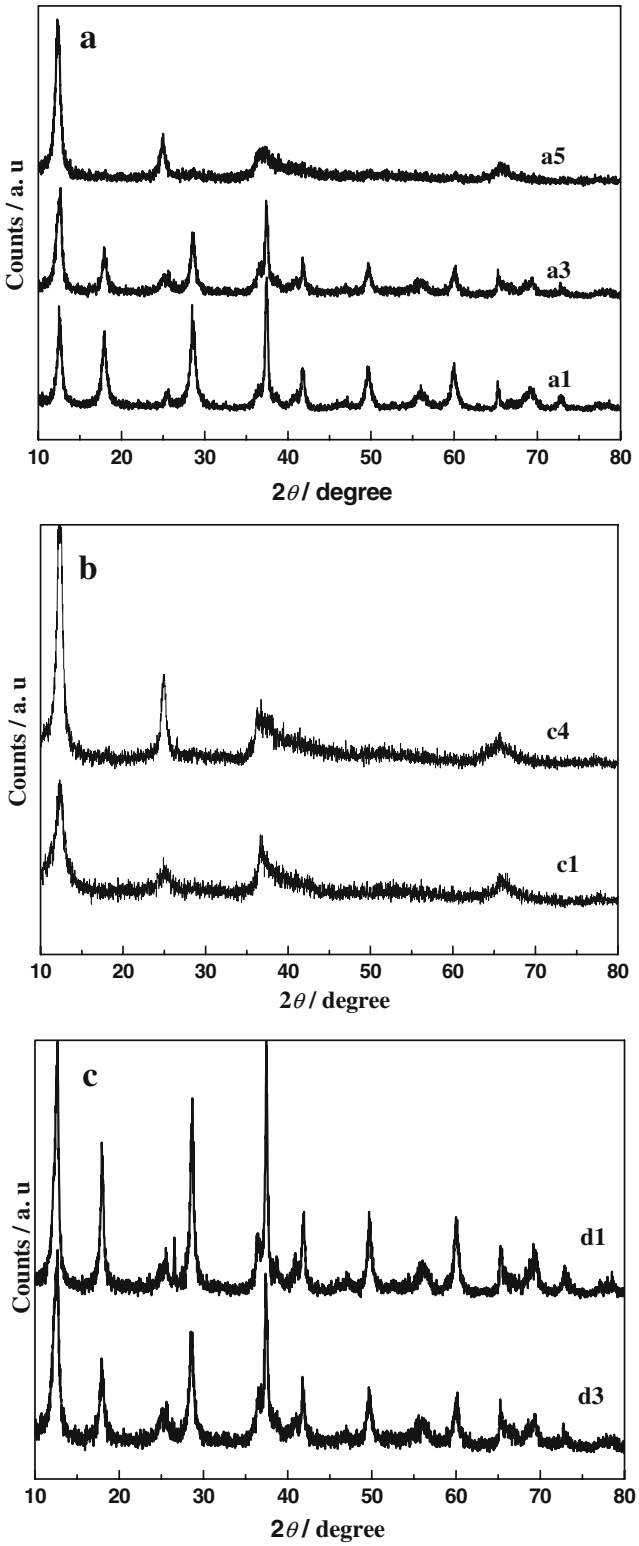

Fig. 1 XRD patterns of MnO_2 materials derived from different synthetical conditions. **a** The molar ratio of $KMnO_4/MnSO_4$ at 1:1, 2:1, and 3:1; **b** the reaction temperature at 120 or 140°C; **c** the reaction lasted for 2 or 14 h

respectively. The characteristic peaks of both samples appear at 12.5°, 17.9°, 28.7°, 37.4°, 41.8°, 49.6°, and 59.9°. These peaks can be indexed to a pure tetragonal phase [space group, $I4/m(87)$] of α-MnO_2 (JCPDS44-0141). It is also observed that the intensity of diffraction peaks for sample prepared by 1:1 molar ratio of reactant is stronger and sharper than that by 2:1 molar ratio of reactant. This shows that the crystalline degree of a1 sample is higher, and the grain size is larger. The average size of sample a1 and a3 calculated from the Scherrer's equation is 16.3 and 12.6 nm, respectively. When the molar ratio of $KMnO_4/MnSO_4$ is 3:1, the diffraction pattern of prepared MnO_2 is largely different compared with the other two, the diffraction peaks appear at 12.3°, 24.9°, 36.6°, and 65.8°. All the diffraction peaks were indexed to a pure rhombic phase [space group R-$3m(166)$] of layered δ-MnO_2 (JCPDS52-0556). It is a hydrated MnO_2 containing K^+, and the chemistry general formula is $K_{0.27}MnO_2{\cdot}0.54H_2O$ [2, 15]. The average size is estimated to be 11.9 nm according to the Scherrer's equation.

Figure 1b and c shows the XRD patterns of MnO_2 obtained at different temperatures and reaction time, respectively. As shown in Fig. 1b, XRD patterns of the samples obtained at different temperatures correspond to well crystallize single-phase α-MnO_2 when the reactant molar ratio of $KMnO_4/MnSO_4$ is 2:1. However, when the reactant molar ratio is 3:1 and the filling factor is increased to 90%, with hydrothermal reaction time changing, all diffraction peaks of both samples are attributable to the layered δ-MnO_2 phase in agreement with the standard spectrum (JCPDS52-0556). It can be seen from the figure that the diffraction peaks of sample obtained at 2 h or 120°C is slightly weaker than that of sample obtained at 14 h or 140°C. This result reveals that the crystalline degree of MnO_2 becomes weaker when the reaction time for hydrothermal process is shorter. However, the crystalline degree of MnO_2 obtained at high temperature is higher. The α-MnO_2 (200) (2θ=17.9º) and δ-MnO_2 (002) (2θ=24.9º) peaks were used to calculate the particle size of α-MnO_2 and δ-MnO_2 according to the Scherrer's equation, respectively. The average size of α-MnO_2 obtained at 2 and 14 h is estimated to be 8.3 and 12.6 nm, respectively. However, the average size of δ-MnO_2 prepared at 120 and 140°C is estimated to be 12.6 and 17.3 nm, respectively. Comparing synthetical conditions with XRD results, we can find that the crystallographic structure of MnO_2 is influenced by the reactant molar ratio. At the same reactant molar ratio, the reaction time and temperature has a very important influence on the average size of MnO_2.

TEM studies

Figure 2 shows a typical TEM image of MnO_2 obtained on the condition that the molar ratio of $KMnO_4/MnSO_4$ is 1:1, 2:1 and 3:1, respectively. As revealed by Fig. 2, when the

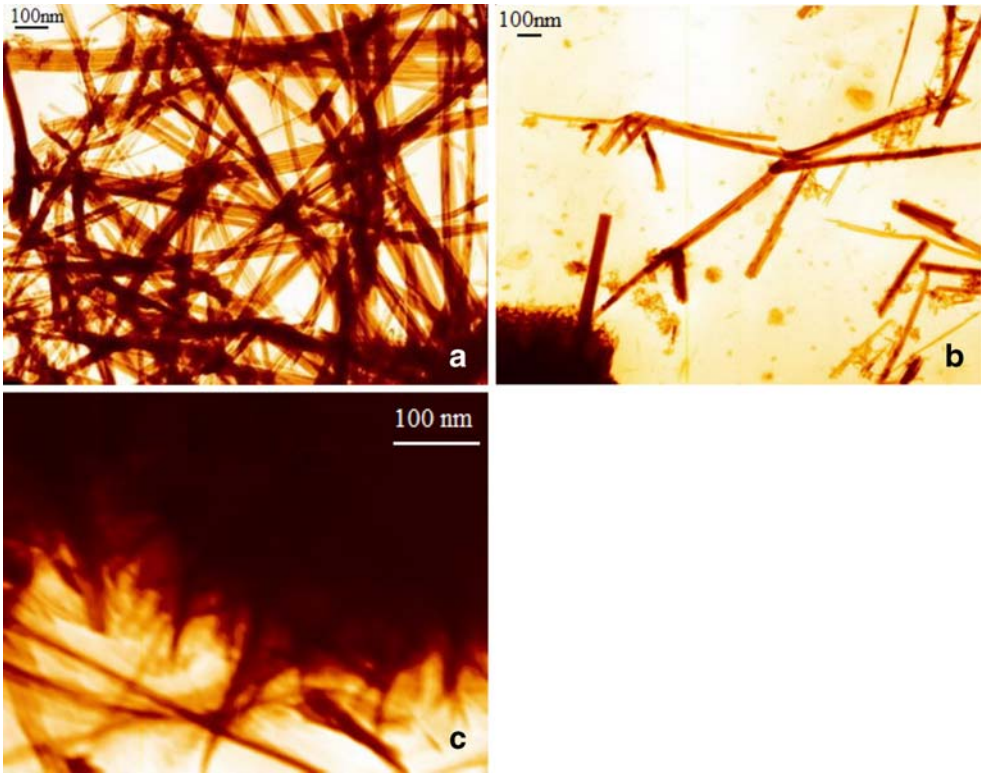

Fig. 2 TEM image of sample a1 (**a**), a3 (**b**), and a5 (**c**)

molar ratio of $KMnO_4/MnSO_4$ is 1:1, the obtained MnO_2 shows a rod-like morphology. The diameter of nanorods is about 20–30 nm, and the length is about 1 μm. When the molar ratio of $KMnO_4/MnSO_4$ is 2:1, the morphology of sample is various. We can observe the longer 1D nanorods, shorter nanorods, fine whiskers, and small amount fine particle (Fig. 2b). The δ-MnO_2 sample, synthesized with the molar ratio of $KMnO_4/MnSO_4$=3:1, is composed of agglomerate petal-shaped thin nanosheet (dark part in Fig. 2c). In the bottom of TEM image, the 1D rod-like structure in the nanoscale has been observed. Maintaining the molar ratio of $KMnO_4/MnSO_4$ at 3:1, the filling factor is increased to 90%. When the hydrothermal dwell time is shorter (2 h), the petal-shaped thin nanosheet in δ-MnO_2 is small, and the agglomerate structure is dense (see Fig. 3a). The largely agglomerated nanowhiskers show an increase in density and tend to loosen as the hydrothermal dwell time increases (14 h), and some grow into nanosheets. At the same time, the rod-like architectures with large size appear (see Fig. 3b–d). This phenomenon is consistent with the reports by Subramania et al. [9] that the MnO_2 with different nanoarchitectures can be synthesized by varying the hydrothermal reaction time.

Electrochemical properties

Figure 4 shows the cyclic voltammogram of MnO_2 prepared at different condition in aqueous 0.5 mol L^{-1} Na_2SO_4 electrolyte. The potential range is from −0.2 to 1.0 V (vs. SCE) and the scanning rate is 5 mV s^{-1}. It can be seen that the synthesized MnO_2 possesses typical pseudo-capacitance properties within −0.1–0.85 V (vs. SCE). The value of current response is almost constant. It is almost symmetric between the cathode process and anode process within −0.1–0.85 V (vs. SCE), which indicates the good reversibility of the MnO_2 electrode within −0.1–0.85 V (vs. SCE). When the scanning direction is changed, the MnO_2 electrode quickly produces current response, and the current immediately changes its flow direction. These results indicate that the internal resistance is very low [16]. The voltammogram suggests that the current values for the α-MnO_2 electrode, obtained on the condition that the molar ratio of $KMnO_4$ to $MnSO_4$ is low, are very low. The sharp peak at both ends of potential window is very large.

The galvanostatic charge–discharge behavior of MnO_2 prepared under different condition was investigated in 0.5 mol L^{-1} Na_2SO_4 solution at 70 mA g^{-1}. These constant current charge–discharge curves are shown in Fig. 5. A good linear variation of potential vs. time was observed in all curves, which is another typical characteristic of an ideal capacitor. During the charging and discharging steps, the charge curves are very symmetric to their corresponding discharge counterparts in the whole potential region, which implies high reversibility and high Coulombic efficiency [3]. It also can be seen that the charge and discharge time of α-MnO_2 decreases with the molar ratio decreasing, viz., the capacitance of α-MnO_2 is lower.

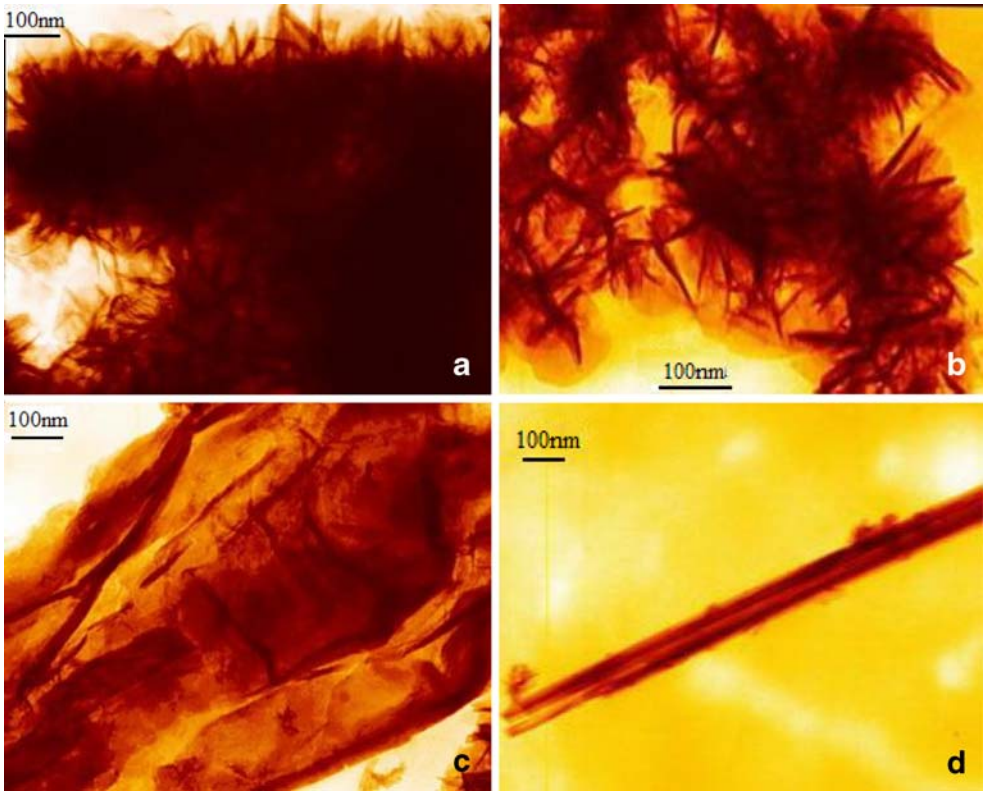

Fig. 3 TEM image of sample c1 (**a**) and c4 (**b**–**d**)

In order to investigate the effect of reactant molar ratio [$n(KMnO_4)/n(MnSO_4)$] on the performance of MnO_2 sample, the galvanostatic charge–discharge behavior of MnO_2 (a1–a5) was studied in 0.5 mol L^{-1} Na_2SO_4. Then, the specific capacitance of each sample is calculated according to Eq. 1. Dependence of the specific capacitance of MnO_2 on the initial molar ratio of reactant is shown in Fig. 6. It can also be seen from Fig. 6 that the specific capacitance of MnO_2 gradually increases with the initial molar ratio of reactants increasing.

Figure 7 presents the specific capacitance of MnO_2 obtained at different hydrothermal dwell time when the molar ratio of $KMnO_4/MnSO_4$ is 2:1 (the samples are b1–b5) and 3:1 (the samples are c1–c4), respectively. It can be seen that the specific capacitance of MnO_2 decrease with increasing reaction time at different molar ratios. When the molar ratio of $KMnO_4$ to $MnSO_4$ is 3:1, the decreasing rate of specific capacitance for MnO_2 is slower with increasing reaction time. The specific capacitance of MnO_2 obtained in hydrothermal reaction for 2 and 14 h is 259.19 and 191.03 $F g^{-1}$, respectively.

During the hydrothermal reaction, the pressure formed at different temperatures in a synthetic system varied; therefore, the environment of obtaining products is different. In our work, the effect of reaction temperature on the performance of MnO_2 was investigated. Table 1 listed the specific capacitance of sample obtained at different hydrothermal temperatures. As can be observed from Table 1, the specific capacitance of final products decreased from 122.19 to 85.57 $F g^{-1}$ with increasing reaction temperature from 120 to 140 °C. This result reveals that the specific capacitance of MnO_2 decreases with the increase of reaction temperature and the decreasing rate is quick.

Discussion

Crystallographic structure and morphology of MnO_2

Through the above experimental results, it can be seen that the controlling crystallographic structure of MnO_2 can be achieved by altering the molar ratio of $KMnO_4/MnSO_4$. This conclusion is consistent with the reports by Wang et al. [17] that the δ-MnO_2 can be produced at a higher K^+ concentration. This phenomenon appeared probably due to the following reasons [17].

The aqueous solution of $KMnO_4$ and $MnSO_4$ was used to carry out hydrothermal reaction, and the whole reaction is given in Eq. 2:

$$2KMnO_4 + 3MnSO_4 + 2H_2O \rightarrow 5MnO_2 + K_2SO_4 + 2H_2SO_4. \quad (2)$$

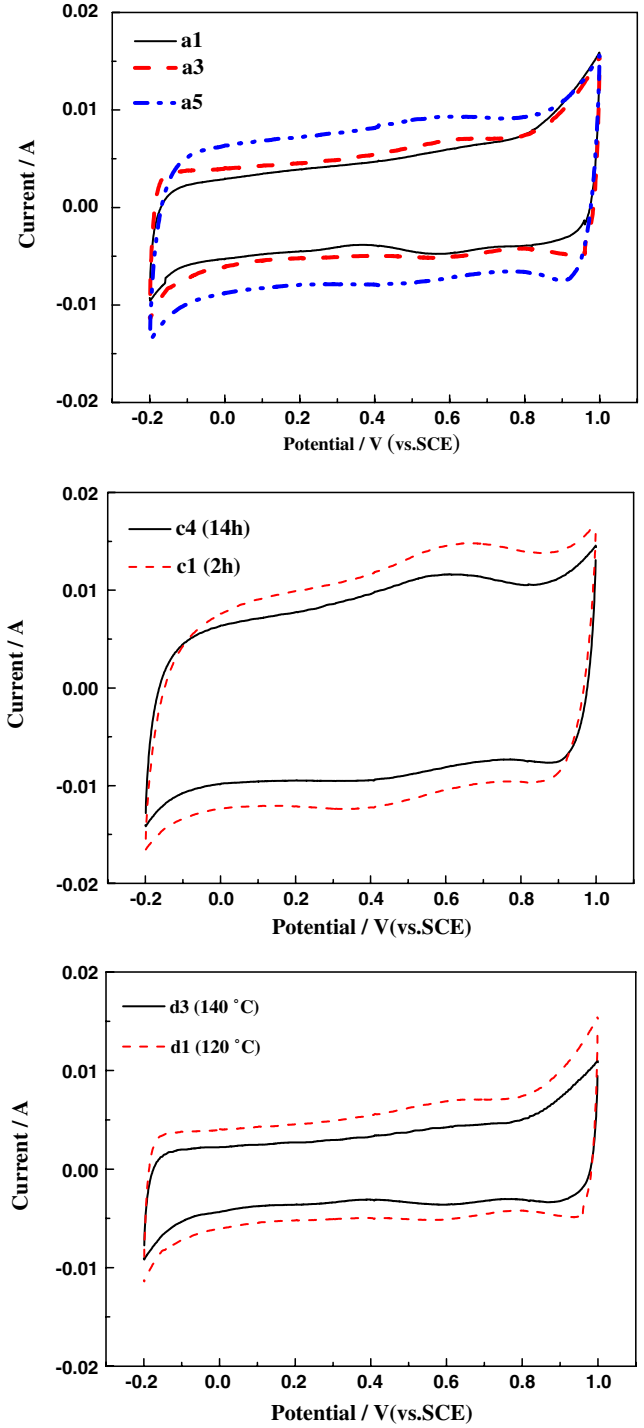

Fig. 4 Cyclic voltammograms of MnO_2 nanostructures prepared at different synthetical conditions recorded at a scan rate of 5 mV s^{-1} in a 0.5 mol L^{-1} Na_2SO_4 aqueous electrolyte

On the other hand, $KMnO_4$ decomposes in solution; therefore we get Eq. 3:

$$KMnO_4 + [(1 - x + 2y)/2]H_2O \rightarrow K_xMnO_2yH_2O + (1 - x)KOH + [(3 + x)/4]O_2 \quad (3)$$

In hydrothermal reaction, the α-MnO_2 can be obtained by Eq. 2. Wang et al. [17] reported that the XRD patterns of δ-MnO_2 as intermediates have been obtained in the formation process of α-MnO_2. Therefore, the reaction 3 takes place first. However, when a low amount of K^+ exist, the layer structure will directly and quickly collapse into

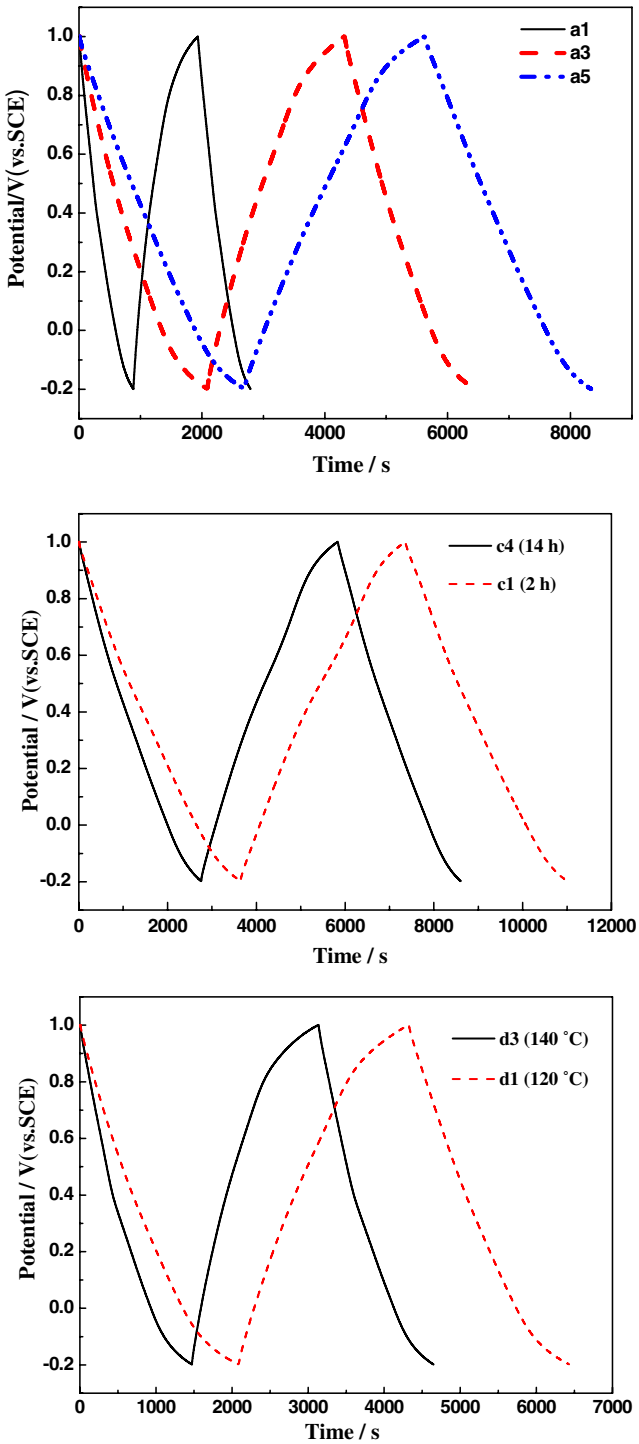

Fig. 5 Galvanostatic charge–discharge behavior of MnO_2 prepared under different condition recorded at a constant current of 70 mA g^{-1}

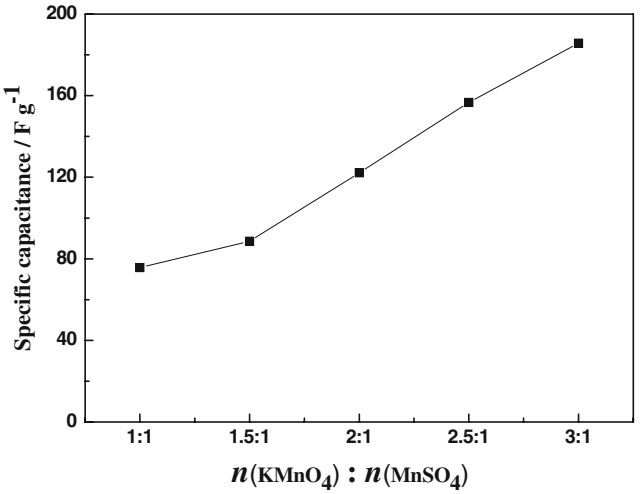

Fig. 6 Dependence of the specific capacitance of MnO_2 (a1–a5) on the initial molar ratio of reactant in 0.5 mol $L^{-1}Na_2SO_4$ at a constant current of 70 mA g^{-1}

(2×2) tunnel formation process of α-MnO_2. In addition, Eq. 2 occurs when the molar ratio of $KMnO_4/MnSO_4$ is lower [12]; therefore, the α-MnO_2 with (2×2) tunnels was obtained on the condition that the molar ratio of $KMnO_4/MnSO_4$ is 1:1 and 2:1. In the reaction, molar ratio of 1:1 is much more beneficial to the conduction of reaction 2. Therefore, the crystalline degree of sample a1 is higher than that of sample a3. At a higher molar ratio, mainly the reaction 3 took place and $K_xMnO_2{\cdot}yH_2O$ was produced. Therefore, in our work, the layered δ-MnO_2 containing K^+ was obtained at the molar ratio of 3:1.

The previous research [9] shows that the MnO_x units will appear first in the solution under hydrothermal conditions, and then they will form sheets of δ-MnO_2 through a condensation reaction. The layered structure δ-MnO_2 is in a metastable state and can maintain its structure with enough cation ions, such as coexistent K^+ [12]. Therefore, when the molar ratio of $KMnO_4/MnSO_4$ is 3:1, the final product is δ-MnO_2 with layered structure. When there are not enough cations, the layer structure will collapse into T(2×2) tunnel structure of α-MnO_2. So the samples of a1 and a3 are α-MnO_2. Compared with sample a1, the small size of crystal grain and high crystalline degree for sample a3 is likely because that the concentration of coexistent K^+ is more than that at a molar ratio of 1:1.

The morphology of MnO_2 changes with varying reaction time at a given molar ratio of reactant. In hydrothermal reaction, the rule of MnO_2 morphology changing is as follows [9]: The MnO_x units will appear first in the solution, and then through a condensation reaction, they will form sheets of δ-MnO_2. After a further prolonged reaction time, the small agglomerate nanoflowers are formed. When the reaction keeps going, these nanosheets like flower gradually grow, and the agglomerates become loose. A subsequent growth leads to the formation of a sheetlike structure. In order to decrease the surface energy, these nanosheets tends to curl and form tubelike structure. Then, tubelike structure gradually forms nanorod structure. Therefore, the MnO_2 with different morphology are displayed in Fig. 3.

Electrochemical behaviors of MnO_2

Specific capacitance, which reflects the charge storage capability per unit mass of electroactive species, is a very important concern for a supercapacitor electrode. The physical factors, such as microstructure, surface area, and the chemical factors, such as valence state and hydrous state, may significantly affect the value of specific capacitance [18–20]. In our work, the optimal synthetic conditions are as follows: The initial molar ratio of $KMnO_4/MnSO_4$ is 3:1, the reaction lasts for 2 h at 120°C, and the filling factor is 90% (the morphology of sample c1 is shown in Fig. 4). In this prepared condition, the MnO_2 with the maximum specific capacitance can be obtained. Prepared δ-MnO_2 has a good layer structure and exhibits nanoflower morphology. The XRD result indicates that the crystalline degree of this sample is lower, and the average grain size is about 8.3 nm. We believe that the specific capacitance of this sample is higher than that of MnO_2 obtained under other conditions due to the effect of crystallographic structure, morphology, and small grain size. The effect of crystallographic structure is concerned with the mechanism of electrochemical reaction for MnO_2. There are two charge storage mechanisms on the MnO_2-based electrode [21–23]. The first one is based on the

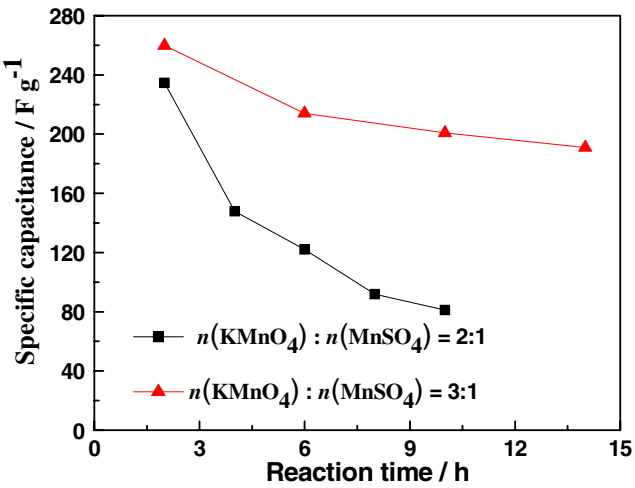

Fig. 7 Dependence of the specific capacitance of MnO_2 on hydrothermal dwell time in 0.5 mol L^{-1} Na_2SO_4 at a constant current of 70 mA g^{-1}. The molar ratio of $KMnO_4$ to $MnSO_4$ is 2:1 (**a**) and 3:1 (**b**), respectively

Table 1 Specific capacitances of MnO_2 prepared at different temperatures

Sample	d1	d2	d3
Temperature of hydrothermal reaction (°C)	120	130	140
Specific capacitance (F g^{-1})	122.19	100.60	85.57

concept of intercalation of H^+ or alkali metal cations, such as Na^+ in the electrode during reduction and deintercalation upon oxidation

$$MnO_2 + C^+ + e \leftrightarrows MnOOC^+ \quad (4)$$

The second one is the adsorption of cations in the electrolyte on the MnO_2 electrode

$$(MnO_2)_{surface} + C^+ + e \leftrightarrows \left(MnO_2^- C^+\right)_{surface} \quad (5)$$

Therefore, the structure, which is beneficial to intercalation and deintercalation of H^+ or Na^+, may be in favor of enhancing specific capacitance. In present reports [12, 30], it was generally believed that δ-MnO_2 is a 2D-layered structure with an interlayer separation of ~7 Å [24]. It has a significant amount of water and stabilizing cations such as Na^+ or K^+ between the sheets of MnO_6 octahedra [12, 30], and the open-layered structure can accommodate alkali ions in its bulk. The α-MnO_2 is 1D (2×2) tunnel structure. The size of the (2×2) tunnel is ~4.6 Å, which is suitable for insertion/extraction of alkali cations [25]. A small amount of cations, such as Na^+, K^+, or H_3O^+ is required to stabilize the (2×2) tunnels in the formation of α-MnO_2 [12, 30]. This conclusion has been given from following facts: (1) The previous report [2] shows that the α-MnO_2 is a lack of potassium compared to the standard cryptomelane phase. The resulting formula of α-MnO_2 can be express by $K_{0.05}MnO_2H_{0.10}$. However, the formula of δ-MnO_2 is $K_xMnO_2H_{0.10}$ (x=0.20–0.3) [15]. (2) In most of the previously reported, it is found that the α-MnO_2 tends to be stable in aqueous concentrated acid [26–28], so the concentration of coexistent H^+ is more. δ-MnO_2 with layered structure exists preferential in aqueous concentrated base [29], and cations is necessary to stabilize the structure of layered compounds; therefore, the concentration of coexistent K^+ is more than that of α-MnO_2.

However, the K^+ of large size possesses certain space, and the diffusion of Na^+ and H^+ into the bulk of MnO_2 is prevented. Thus, in Fig. 7, the specific capacitance of MnO_2 obtained at 2:1 reactant molar ratio is far less than that of MnO_2 obtained at 3:1 molar ratio. The crystalline degree of products increases with prolonging the hydrothermal reaction time. At the same time, the amount of hydration water decreases, and the content of K^+ in tunnel structure of α-MnO_2 increases. Therefore, the specific capacitance of α-MnO_2 decreases with the increase of hydrothermal dwell time and has a rapid descent rate.

Ghodbane et al. [30] reported that the specific surface area has a limited impact on the capacitance of MnO_2-based electrodes. Devaral et al. investigated the effect of crystallographic structure of MnO_2 on its electrochemical capacitance properties [12]. In their report, the specific capacitance of α-MnO_2 is 297 F g^{-1} at a constant current of 1 A g^{-1}. However, in our work, the specific capacitance of sample a1 and a3 is 80 and 120 F g^{-1} at discharge current of 70 mA g^{-1}, respectively. The α-MnO_2 obtained by Devaral et al. [12] is agglomerate composed of zero-dimensional particles, and the morphology is other than that of the 1D nanorod α-MnO_2. In many electrochemical reactions, the reactive properties of nanostructure depend strongly on their size, shape, and chemical composition, among which the shape of a nanostructure determines its surface atomic arrangement and coordination [31]. In other words, in our work, the capacitance performance of MnO_2 is not only closely related to crystallographic structure but also to morphology and grain size. As mentioned above, under the condition of low molar ratio, long hydrothermal dwell time, and high reaction temperature, the sample with large grain and small active site of electrochemical reaction was obtained. Due to its small specific area and small active site of electrochemical reaction, the specific capacitance is lower. When the product are obtained under the condition of high molar ratio, short hydrothermal dwell time, and low reaction temperature, the specific capacitance increases with gain size of products decreasing. As sample is layered δ-MnO_2, the effect of hydrothermal dwell time on the capacitance performance is relatively small. Thereby, it can be seen from Fig. 7 that the specific capacitance is slowly dropped with increasing reaction time.

Conclusion

Nanostructure MnO_2 samples with two different crystal structures were synthesized under hydrothermal condition, and they were investigated as electrode materials for electrochemical capacitors in aqueous 0.5 mol L^{-1} Na_2SO_4 solution. The XRD, TEM, CVs, and galvanostatic charge–discharge studies showed that the major product was α-MnO_2 with (2×2) tunnels at low initial molar ratio of reactant. At a higher molar ratio of $KMnO_4$ to $MnSO_4$, the major product is layered δ-MnO_2. The capacitance performance of latter is superior because the layered structure is beneficial to insertion/extraction of H^+ or Na^+. When the product were

obtained under the condition of high molar ratio, short hydrothermal dwell time, and low reaction temperature, the specific capacitance increased with morphology changing and gain size of products decreasing. This was due to that the specific capacitance of MnO_2 was affected by crystallographic structure, morphology, and gain size. In the present study, layered δ-MnO_2 prepared hydrothermally at 120 °C for 2 h showed the best performance with a specific capacitance of 259.19 F g^{-1} at a constant current of 70 mA g^{-1}. Further work is to investigate the effect of long cycle performance on the electrode structure and associate the structural changes with impedance changes.

Acknowledgment Financial support for this work was provided by Major State Basic Research Development Program (no. 2008CB617502).

References

1. Chu A, Braatz P (2002) J Power Sources 112:236
2. Toupin M, Brousse T, Bélanger D (2002) Chem Mater 14:3946
3. Xu C, Li B, Du H, Kang F, Zeng Y (2008) J Power Sources 180:664
4. Subramanian V, Zhu H, Wei B (2008) Chem Phys Lett 453:242
5. Yuan A, Wang X, Wang Y, Hu J (2009) Electrochim Acta 54:1021
6. Zolfaghari A, Ataherian F, Ghaemi M, Gholami A (2007) Electrochim Acta 52:2806
7. Yan D, Yan P, Cheng S, Chen J, Zhuo R, Feng J, Zhang G (2009) Cryst Growth Des 1:218
8. Chen X, Li X, Jiang Y, Shi C, Li X (2005) Solid State Commun 136:94
9. Subramanian V, Zhu H, Vojtal R, Ajayan PM, Wei B (2005) J Phys Chem B 109:20207
10. Ding Y, Shen X, Gomez S, Luo H, Aindow M, Suib SL (2006) Adv Funct Mater 16:549
11. Xu M, Kong L, Zhou W, Li H (2007) J Phys Chem C 111:19141
12. Devaraj S, Munichandraiah N (2008) J Phys Chem C 112:4406
13. Athoul L, Moser F, Dugas R, Crosnier O, Blanger D, Brousse T (2008) J Phys Chem C 112:7270
14. Ni J, Lu W, Zhang L, Yue B, Shang X, Lv Y (2009) J Phys Chem C 113:54
15. Chen R, Zavalij P, Whittingham MS (1996) Chem Meter 8:1275
16. Chang JK, Huang CH, Lee MT, Tsai WT, Deng MJ, Sun IW (2009) Electrochim. Acta 54:3278
17. Wang X, Li YD (2003) Chem Eur 9:300
18. Beaudrouet E, Salle ALGL, Guyomard D (2009) Electrochim Acta 54:1240
19. Wei W, Cui X, Chen W, Ivey DG (2009) J Power Sources 186:543
20. Ghaemi M, Ataherian F, Zolfaghari A, Jafari SM (2008) Electrochim Acta 53:4607
21. Pang SC, Anderson MA, Chapman TW (2000) J Electrochem Soc 147:444
22. Kuo SL, Wu NL (2006) J Electrochem Soc 153:A1317
23. Toupin M, Brousse T, Belanger D (2004) Chem Mater 16:3184
24. Ma R, Bando Y, Zhang L, Sasaki T (2004) Adv Mater 16:918
25. Reddy RN, Reddy RG (2003) J Power Sources 124:330
26. Kijima N, Yasuda H, Sato T, Yoshimura Y (2001) J Solid State Chem 159:94
27. Xiao TD, Strutt PR, Benaissa M, Chen H, Kear BH (1998) Nanostruct Mater 10:1051
28. DeGuzman RN, Shen YF, Neth EJ, Suib SL, O'Young CL, Levine S, Newsam JM (1994) Chem Mater 6:815
29. Luo J, Suib SL (1997) J Phys Chem B 101:10403
30. Ghodbane O, Pascal JL, Favier F (2009) Appl Mater Interfaces 1 (5):1130
31. Tian N, Zhou ZY, Sun SG (2008) J Phys Chem C 112:19801